Frontiers of Environmental Science & Engineering
2025, 19(6): 82 https://doi.org/10.1007/s11783-025-2002-y

RESEARCH ARTICLE

Insights into seasonal temperature shifts on a robust composite-substrate autotrophic denitrification reactor for treating municipal secondary effluent

Chuanyi Zhang[1], Zhiping Zhu[1], Limei Yuan[1], Daxin Yang[1], Qiang Xu[2], Sijie Ge ✉ [1,2]

1. School of Environment Science and Spatial Informatics, China University of Mining and Technology, Xuzhou 221116, China
2. Dan F. Smith Department of Chemical & Biomolecular Engineering, Lamar University, Beaumont, TX 77710, USA

HIGHLIGHTS

- A robust reactor resistance to low temperature was developed for N and P removal.
- NRL of 0.032 kg NO_3^--N /(m^3·d) and NRE of 30.2% were achieved at 10.4 °C.
- *Thiobacillus* was enriched and the predominant genera serving for denitrification.
- Feasibility and merit of SPSAD were demonstrated in municipal secondary effluent.

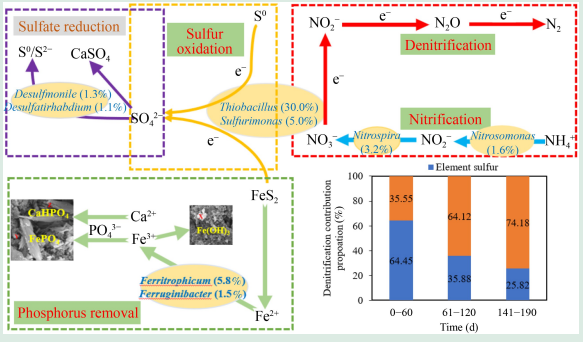

ABSTRACT: Sulfur autotrophic denitrification (SAD) is a promising biological nitrogen removal technology without CO_2 emissions. However, the impact of seasonal temperature variations on SAD performance, especially in the treatment of actual municipal secondary effluent, remains unclear. To address this issue, a composite substrate SAD reactor (i.e., SPSAD), where element S^0 and pyrite (v:v/1:3) were uniformly mixed in hollow plastic balls that served as the filler, was developed in this paper. The performance of the SPSAD reactor was comprehensively evaluated under 190 d of seasonal variation. The results indicated that the nitrate removal loading (NRL), nitrate removal efficiency (NRE), and PO_4^{3-}-P removal rate decreased from 0.060 kg NO_3^--N /(m^3·d), 93.2% and 67.9% to 0.032 kg NO_3^--N /(m^3·d), 49.9% and 30.2%, respectively, when the temperature decreased from 35 °C to 9 °C. The SPSAD reactor was effective at performing denitrification under temperature variations. Additionally, the ratio of ΔSO_4^{2-} to ΔNO_3^--N gradually decreased from 6.48 to 5.34 as the temperature decreased, revealing a shift in the predominant electron donor for denitrification from S^0 to pyrite. Microbial analysis revealed that the average abundance of *Proteobacteria* was 53.11%, making it the dominant phylum in the reactor. *Thiobacillus* was significantly enriched as the predominant genus responsible for denitrification, with its abundance decreasing from 33.2% at Stage I (25–35 °C) to 26.4% at Stage III (9–11 °C). The feasibility and advantages of NO_3^--N and PO_4^{3-}-P removal via the SPSAD reactor were discussed and demonstrated in practical applications. This study provides stakeholders with

✉ Corresponding author. E-mail: gesijie@cumt.edu.cn
Article history: Received 1 December 2024, Revised 24 February 2025, Accepted 1 April 2025, Available online 20 April 2025

scientific support for the deep treatment of municipal secondary effluent in cold areas.

KEYWORDS: Sulfur Autotrophic, NO_3^--N, PO_4^{3-}-P, Seasonal Temperature, Secondary effluent

1 Introduction

The excessive discharge of nitrogen and phosphorus nutrients into water bodies is a root cause of eutrophication. Sulfur autotrophic denitrification (SAD), a promising alternative nitrogen removal technology, has become a research hotspot in autotrophic denitrification over the past several decades (Sahinkaya et al., 2011; Wang et al., 2023; Shi et al., 2024). Compared to conventional heterotrophic denitrification, SAD exhibits several benefits, such as organic carbon savings, low sludge production, low operation costs, and decreased greenhouse gas emissions (e.g., CO_2) (Cui et al., 2024; Wang et al., 2024). SAD technologies usually employ the reduced element of sulfur (S^0) or inorganic sulfur compounds (e.g., $S_2O_3^{2-}$, FeS_2) as electron donors to convert electron acceptors of nitrate (NO_3^--N) or nitrite (NO_2^--N) to nitrogen gas (N_2). If element sulfur or inorganic sulfur compounds were utilized as electron donors, the employed SAD reactors would generate large quantities of SO_4^{2-} and fail to efficiently remove phosphorus (). Previous studies report that pyrite can be utilized as an electron donor in SAD reactors, which might reduce effluent SO_4^{2-} generation and avoid the risk of black-odor water bodies (Sahinkaya et al., 2011; Chen et al., 2022). Additionally, the reactor is able to simultaneously accomplish denitrification and phosphorus removal because the Fe^{2+} or Fe^{3+} released from pyrite reacts with phosphorus to form precipitates of phosphorus-containing compounds (Liu et al., 2021). However, there are several disadvantages to the reactor filled with pyrite, such as low denitrification rate, long start-up time, and an increase in alkalinity that results in a pH change of the reactor (Liu et al., 2023). Considering these challenges, there is an urgent need to explore and construct a composite medium reactor (e.g., filled with both the element sulfur and inorganic sulfur compounds) to solve the above contradictions and conflicts.

Recently, several studies investigated the construction of a complex sulfur-based reactor for nitrogen and phosphorus removal. Li et al. (2020a) employed pyrrhotite and sulfur particles as electron donors to establish a composite medium denitrification reactor to treat synthetic secondary effluent, which resulted in effluent NO_3^--N and PO_4^{3-}-P concentrations of less than 0.28 ± 0.14 and 0.01 mg/L, respectively. Additionally, Li et al. (2020b) employed sulfur and pyrite as composite fillers and explored the effects of DO (1.2–1.5 mg/L) on simultaneous NO_3^--N and PO_4^{3-}-P removal from secondary effluent. Chen et al. (2023) constructed an autotrophic denitrification reactor with elemental sulfur/pyrite to investigate the effects of different HRT and P/S ratios on the performance of the reactor, which produced effluent TN and PO_4^{3-}-P concentrations (under HRT = 3 h, P/S = 2–1) of 1.4 and 0.19 mg/L, respectively. Liu et al. (2023) employed static batch tests to investigate the effects of different pyrite on the performance of a composite medium reactor (sulfur/pyrite = 1:1). Lu (2020) examined three composite medium reactors by combining S^0 with one ore (i.e., FeS, $Fe_{1-x}S$ or FeS_2) and recorded the denitrification and phosphorus removal characteristics of the reactor during start-up as well as under different HRT conditions. However, the above studies were carried out at a fixed optimum temperature (approximately 28–30 °C). Notably, the composite medium reactor is affected not only by HRT, P/S, DO, and other factors mentioned above but also by temperature variation, which is a significant challenge to real-world applications.

Temperature is a crucial obstacle to achieving the efficient and stable operation of SAD because temperature significantly affects the metabolic activities of microorganisms (Panswad et al., 2003; Lin et al., 2016; Hu et al., 2019; Meynet et al., 2024). The optimum denitrification temperature of *Thiobacillus* ranged between 25–35 °C, and the denitrification rate rapidly declined to 1/3 of the original rate for every 10 °C decrease (Di Capua et al., 2016). Therefore, low temperatures adversely affect the activity of sulfur autotrophs, posing a significant challenge for biological nitrogen removal processes, particularly during the wintertime. It is essential to develop a robust reactor capable of achieving efficient nitrogen removal under low temperature conditions. Fajardo et al. (2014) analyzed the effect of temperature on the process of autotrophic denitrification using $S_2O_3^{2-}$ as an electron donor; the removal rate of nitrate nitrogen (NRE) sharply decreased from 95% to 55% as the temperature changed from 35 to 25 °C. However, the temperature range in that study was narrow (a max of 10 °C), and the experiment was discontinuous (two independent temperature points), which was insufficient for

analyzing the reactor's long-time operation and microbial community dynamics. Demir et al. (2021) reported a biogenic sulfur-driven MBR, and the NRE was reduced by 40% as the temperature decreased from 30 to 20 °C. Zhou et al. (2024) reported that the performance of a hydrogen autotrophic denitrification system significantly deteriorated at a temperature of 15 °C, and the NO_2^--N accumulation was remarkably high (> 40 mg/L) in the reactor. Thus, low temperatures are inevitably associated with adverse effects on the SAD system. Temperature is strongly influenced by seasonal fluctuations. However, few reports exist on the treatment of actual municipal secondary effluent using SAD reactors under long-term seasonal temperature variations.

In summary, this study established a SAD reactor with sulfur and pyrite as composite fillers (named SPSAD) to evaluate the impact of temperature variations on NO_3^--N, PO_4^{3-}-P, and SO_4^{2-} as well as microbial diversity in a self-constructed reactor system. The actual secondary effluent of a municipal wastewater treatment plant was processed by the developed SPSAD reactor to demonstrate its feasibility and efficacy in real applications. The main objectives of this study were to (1) determine the operational characterization of SPSAD; (2) distinguish the microbial community succession in SPSAD under seasonal temperature variations (i.e., 9–11, 15–25, and 25–35 °C); and (3) demonstrate the mechanism of denitrification and phosphorus removal by SPSAD. This study provides scientific insights into the SPSAD process for the advanced treatment of nitrogen-containing wastewater at low temperatures.

2 Material and methods

2.1 Up-flow reactor device

The reactor device employed in this study had an effective volume of 170 L and was composed of high-density polyethylene, with a diameter of 70 cm and height of 100 cm, as shown in Fig. 1. The bottom of the reactor was filled with ceramic particles sized 2–4 cm as a supporting layer. The reactor adopted an up-flow mode in which the influent continuously entered from the bottom of the reactor via a peristaltic pump (BT301F, LEADFLUID) and then flowed into the effluent bucket along with the liquid. Based on previous data from the research group, sulfur and crushed pyrite (volume ratio 1:3) (Chen et al., 2023) were uniformly mixed and poured into 8 cm diameter hollow plastic balls to ensure biofilm colonization. The porosity of the filter was approximately 65%. During the stable operation of the system, the sludge at the bottom of the reactor was sampled under three temperature ranges to examine the changes in the microbial community structure. One bioreactor was employed in this study.

2.2 Sludge inoculation and reactor start-up

Sulfur autotrophic denitrifiers were enriched and collected from activated sludge taken from the anoxic tank of the wastewater treatment station (A^2/O process) at the Nanhu Campus of China University of Mining and Technology in Xuzhou, China. The mixed liquid suspended solids (MLSS) concentration of the inoculated sludge was approximately 5000 mg/L. The reactor was inoculated with 120 L of sludge per treatment and was fed water to ensure the effluent water

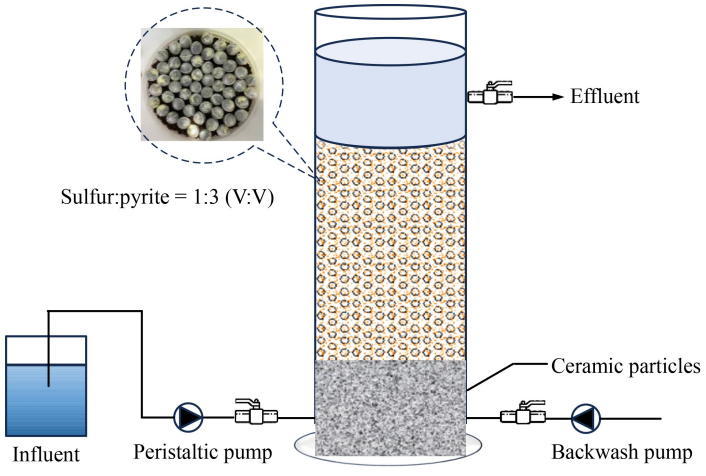

Fig. 1 Schematic diagram of the experimental device.

circulated back into the device. After the biofilm grew on the filler and no obvious sludge floc was observed in the effluent, the operational experiments (i.e., Stage I through III) were initiated. The influent was taken from the actual effluent of the sand filter at the end of the wastewater treatment process. The main parameters of the influent under the three temperature ranges are shown in Table 1. The temperature values reflect the actual room temperature, which varied with the seasons, and the three stages are delineated sequentially according to the temperature range. The experimental device was operated continuously for 226 d, including 36 start-up days. To clearly observe the impact of seasonal temperature on SAD performance, the HRT was set at 12 h with the maximum denitrification rate based on our previous study (Lu, 2020). The influent NO_3^--N concentration during the start-up period was adjusted to 18–22 mg/L and then adjusted to 25 ± 1 mg/L during the three stages by adding additional NO_3^--N to the actual effluent. The removal efficiency of NO_3^--N was stable at 63.2% on 27 d after the reactor was started. Gray-brown sludge flocs gradually appeared and attached to the surface of the packing ball, which indicated that the reactor accomplished biofilm colonization, thus achieving a successful start-up within 27–36 d. After the reactor completed start-up, three stages (starting on the 37th day) of experiments were performed over the following 190 d. The influent concentrations of NH_4^+-N and PO_4^{3-}-P during the three stages were 3–8 and 0.4–0.75 mg/L, respectively. The durations of Stages I, II and III were 60, 60, and 50 d, respectively. On day 120, the sampling analysis of the reactor was stopped for 20 d due to a laboratory shut-down because of a safety-checked restriction. The bioreactor continued to run during this break, with influent parameters similar to Stage II instead of temperature.

2.3 Sampling analysis

The water samples were filtered through a 0.45 μm membrane filter, and the concentrations of NO_3^--N, NO_2^--N, NH_4^+-N, PO_4^{3-}-P, and SO_4^{2-} were measured daily with an ultraviolet spectrophotometer (SP-756P, Spectrum Shanghai, China) according to standard methods. Dissolved oxygen (DO) and pH were measured with a water quality instrument (multi-3320, WTW, Germany). The calculation methods can be found in our previous work (Yang et al., 2024). Scanning electron microscopy (SEM) micrographs were obtained using a field emission scanning electron microscope (Quanta FEG 250, FEI, Czech Republic), and the elemental composition of the particulate samples was measured by an energy dispersive spectrometer (EDS, EDX 4500, EDAX, USA). SEM and EDS were used to determine the form of phosphorus removal, and EDS was used to determine the elemental composition of the samples. Combined with the SEM electron micrographs, it was preliminarily determined that most of the phosphorus removed was in the form of $FePO_4$, which proved that the removal of phosphorus mainly relied on chemical precipitation rather than the adsorption of sulfurous iron ores. Changes in the composition of the microbial communities were sampled at three different temperature ranges and analyzed.

2.4 Microbial community structure analysis

Sludge samples were collected from the reactor at Stages I, II, and III, and then stored at the low temperature of −80 °C in a refrigerator. Majorbio Bio-Pharm Technology Co. Ltd. (Shanghai, China) analyzed the sludge samples to identify the structure of the microbial population. Bacterial DNA was extracted with an E.Z.N.A™ Mag-Bind Soil DNA Kit (M5635-02, OMEGA) according to the manufacturer's protocol. Following PCR amplification, the resulting amplicons were sequenced using Illumina high-throughput sequencing. The V3-V4 region of the bacterial 16SrRNA was amplified using the bacterial primers 338F (5'-ACTCCTACGGGAGGCAGCA-3') and 806R (5'-GACTACHVGGGTWTCTAAT-3'). The sequencing platform was Illumina Miseq/Hiseq PE250. After the OTU data were analyzed for multiple diversity indices, the OTU classification results were plotted against the phylum- and genus-level community abundance maps on the basis of the analytical information.

Table 1 Operational parameters of each stage during the experiment

Stage	Temperature (°C)	Duration (d)	Influent NO_3^--N (mg/L)	Influent NH_4^+-N (mg/L)	Influent PO_4^{3-}-P (mg/L)	HRT (h)
I	25–35	60	25 ± 1	3–8	0.40–0.65	12
II	15–25	60	25 ± 1	3–8	0.50–0.75	12
Break	Undetected	20	25 ± 1	3–8	0.50–0.75	12
III	9–11	50	25 ± 1	3–8	0.51–0.75	12

3 Results and discussion

3.1 Performance of the SPASD reactor

3.1.1 Nitrogen removal performance

The concentrations of influent and effluent NO_3^--N, NO_2^--N, and NH_4^+-N as well as the NRE of the SPSAD reactor varied with temperature, as shown in Fig. 2. The influent NO_3^--N concentration was 25 ± 1 mg/L, and the average effluent NO_3^--N concentrations of Stages I through III were 1.73, 5.93, and 12.60 mg/L, respectively. The average NREs were 93.17%, 76.39%, and 49.94%, respectively. The denitrification performance of the reactor worsened with decreasing temperatures. Denitrification performance was best at Stage I (25–35 °C) and satisfactory at Stage II (15–25 °C), and the overall nitrogen removal performance remained at a high level. The results suggested that the constructed SPSAD reactor exhibited a certain degree of resistance to temperature variations. In comparison to Stages I and II, the denitrification performance at Stage III (9–11 °C) further deteriorated, and the effluent NO_3^--N concentration increased to 12.60 mg/L. As the temperature decreased, both the liquid-phase mass transfer coefficient and the activity of nitrate reductase decreased (Li et al., 2022; Zhou et al., 2024), which hindered the transformation of NO_3^--N to NO_2^--N. Miu et al. (2019) employed the element S^0 as an electron donor to build an SAD reactor and decreased the NRE by 76% at 15 °C and by 96.8% at 5 °C compared to that at 25 °C. Chen et al. (2018) established a reactor that coupled bioelectrochemical processes with SAD, which increased NRE to 54.41% with an applied 50 mA current and 9 h HRT at 10 ± 2 °C. In summary, the constructed SPSAD had a strong resistance to low temperature and maintained a better denitrification performance without additional measures. The overall reactions for element S^0 and pyrite-based denitrification are summarized as follows:

$$55S + 50NO_3^- + 38H_2O + 20CO_2 + 4NH_4^+ \rightarrow 4C_5H_7O_2N + 25N_2 + 55SO_4^{2-} + 64H^+ \quad (1)$$

$$0.364FeS_2 + NO_3^- + 0.821H_2O + 0.023NH_4^+ + 0.116CO_2 \rightarrow 0.023C_5H_7O_2N + 0.5N_2 + 0.729SO_4^{2-} + 0.364Fe(OH)_3 + 0.48H^+ \quad (2)$$

in general, denitrification includes two steps that convert NO_3^--N to N_2. NO_3^--N is first reduced to NO_2^--N by nitrate nitrogen reductase, and then NO_2^--N is further reduced to N_2 by nitrite nitrogen reductase (NirS). No substantial accumulation of NO_2^--N was observed in Stage I (25–35 °C), whereas the accumulation of NO_2^--N increased from 0.34 mg/L at Stage II to 1.10 mg/L at Stage III. This result suggested that the inhibitory effect caused by low temperature on NirS from sulfur autotrophic denitrifying bacteria was stronger than NO_3^--N reductase lineage (Zuo et al., 2024). Zhou et al. (2024) reported that the influent

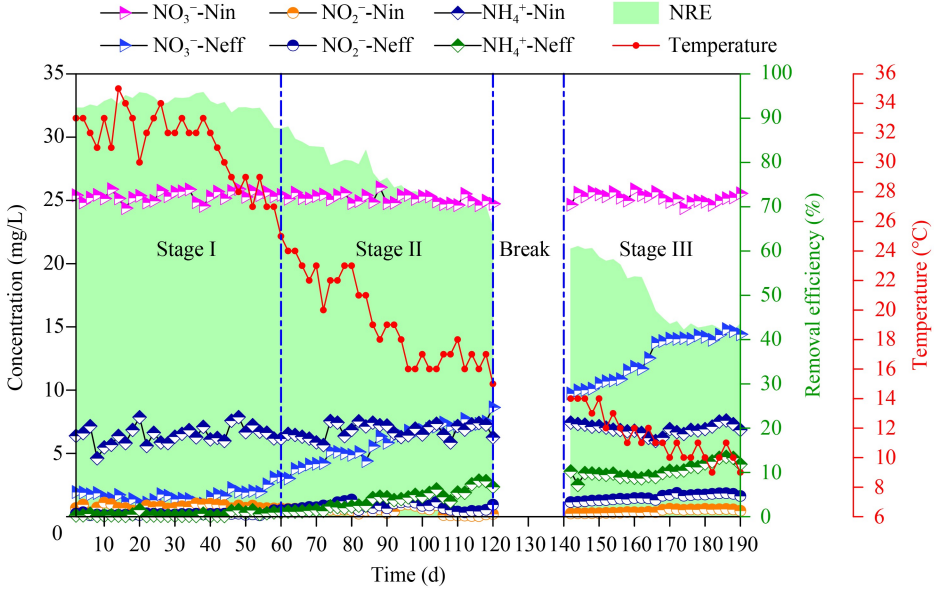

Fig. 2 The concentrations of influent and effluent NO_3^--N, NO_2^--N, and NH_4^+-N, temperature and NRE changed with operating time (total of 190 d) in the SPSAD reactor.

NO_3^--N of a hydrogen autotrophic denitrification system was 100 mg/L, the accumulation of NO_2^--N was 40.3 mg/L, and a 73.7% decrease in the NirS abundance was detected when the temperature was set at 15 °C as opposed to 30 °C.

The removal rate of NH_4^+-N decreased as the temperature decreased. When the reactor proceeded from Stage I to Stage III, the concentration of effluent NH_4^+-N increased from 0.18 to 3.63 mg/L, and the removal rate of NH_4^+-N decreased from 97.30% to 47.57%. Kim et al. (2008) reported that with a free ammonia concentration of 5.6 mg/L, the ammonia oxidation rate was 1.35, 0.85, and 0.2 mg/(L·d) at temperatures of 30, 20, and 10 °C, respectively. Several ammonia-oxidizing microorganisms are fragile and died under the long-term low temperatures, suggesting that large fluctuations in temperature had a significant negative effect on the activities of ammonia-oxidizing bacteria. While NOB has a greater growth rate than AOB in the 10–20 °C range, the growth rate of AOB exceeds that of NOB above 25 °C (Zuo et al., 2024). As such, NOB activity was greater than AOB activity at Stages II and III, and NO_2^--N generated by NH_4^+-N oxidation was able to be completely oxidized to NO_3^--N. A decrease in temperature could have significantly weakened nitrification, slowing the conversion rate of NH_4^+-N (Zhu and Chen, 2002). Given that the effluent NH_4^+-N concentration was always at a low level (< 7 mg/L) in this study, the accumulation of NO_2^--N in Stages II and III could have been caused by the process of transforming NO_3^--N into N_2 via denitrifying bacteria instead of NH_4^+-N conversion via ammonia-oxidizing bacteria.

From Stage I (average temperature 31.1 °C) to Stage III (average temperature 10.4 °C), the nitrate removal loading (NRL) in the reactor decreased from 0.0595 kg NO_3^--N/(m^3·d) to 0.0316 kg NO_3^--N/(m^3·d). The NRL of the SPSAD system appeared to decrease with decreasing temperatures. Li et al. (2020c) investigated the pilot application of a sulfur-limestone autotrophic denitrification biofilter on municipal secondary effluent at low temperatures. The results showed that when the temperature decreased from 20 to 10 °C, the NRE decreased from 74.2% to 52.4%, and the NRL was 0.016 kg NO_3^--N/(m^3·d). Xu et al. (2019) studied the effect of ambient temperature on the denitrification performance of a SAD system using pyrite as an electron donor, resulting in a reduction of NRL from 0.0118 to 0.006 kg NO_3^--N/(m^3·d) (with 15.2% NRE) when the temperature decreased from 28 to 12 °C. Compared to the above studies, the NRL of the SPSAD reactor in this study reached 0.0316 kg NO_3^--N/(m^3·d), with an average temperature of 10.4 °C at Stage III, which confirmed that the SPSAD reactor performed denitrification well at low temperatures.

3.1.2 Phosphorus removal performance

The changes in effluent PO_4^{3-}-P concentrations in the SPSAD reactor due to seasonal temperatures is presented in Fig. 3 and discussed in detail in this section. The concentration of effluent PO_4^{3-}-P gradually increased with decreasing temperature. The average removal efficiency of PO_4^{3-}-P in Stages I, II and III was 68.30%, 40.48%, and 25.31%, respectively. Thus, low temperatures adversely affected PO_4^{3-}-P removal, which is supported by Lv et al. (2024), whose reactor was composed of sulfur-pyrite. Additionally, Li et al. (2024) reported that in a reactor filled with natural magnetic pyrite, the removal rate of PO_4^{3-}-P decreased from 99.1% to 89.8% as the temperature decreased from 29 to 11 °C. This result could be attributed to the following three factors. First, the kinetic energy and diffusion of the iron ions decreased due to the decrease in temperature, which weakened the chance of effective collisions among the ions to form PO_4^{3-}-P precipitation. Second, low temperatures weakened the performance of the SPSAD reactor, which decreased Fe^{2+} production in the reactor. Third, the decrease in temperature significantly affected the activity of iron-oxidizing bacteria (Zhang, 2018), which limited the conversion of Fe^{2+} to Fe^{3+} and reduced the chemical reaction of Fe^{3+} with PO_4^{3-}-P. This was the main reason for the deterioration of phosphorus removal in our SPSAD system.

SEM images of the secondary minerals that formed on the surface of the pyrite ore are shown in Fig. 4. Based on the percentage of atoms characterized by EDS analysis, shown in Table 2, the X position in Fig. 4 was assumed to be an amorphous $Fe(OH)_3$ colloid, which exhibited globular amorphous aggregates with a low degree of crystallinity and was mainly composed of O, Fe and C (Li et al., 2021; Xu et al., 2022). The formation of amorphous $Fe(OH)_3$ agglomerates was possibly due to the adhesion of Fe^{3+} deposits to the microbial cell surface followed by a tight enclosure of the matrix. The high percentage of C (40.16%) at the X position could be due to the high cellular biomass. The secondary minerals marked at the Y and Z positions presented distinct irregular plate-like aggregations with plate lengths of 4–5 μm and widths of 1–2 μm. The elemental compositions of the irregular plate-like aggregations at Y and Z were mainly composed of Fe, P, O, C, and Ca. The P content of the plate-like aggregates accounted for 15.71%–16.44%. The precipitates were recorded as $FePO_4$ and $CaHPO_4$ based

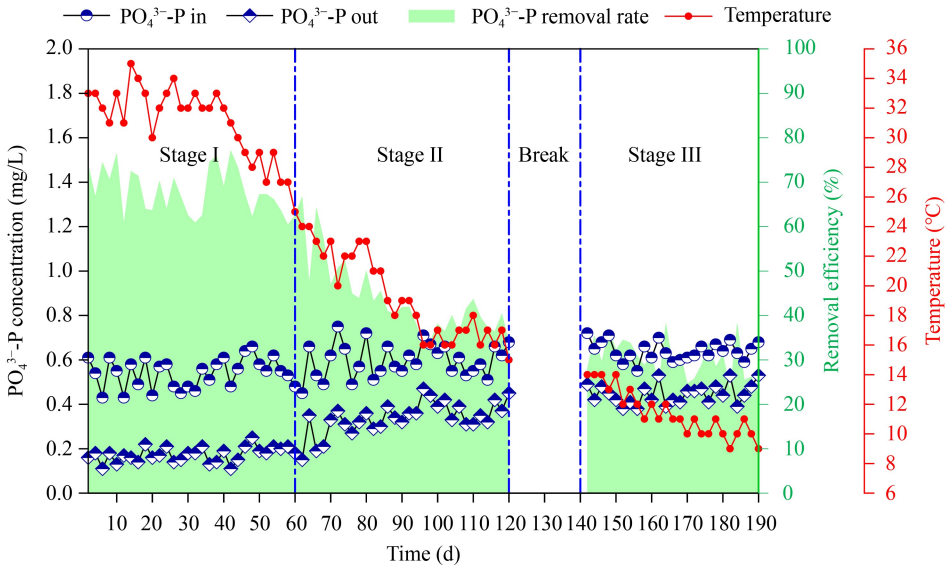

Fig. 3 Effect of seasonal temperature changes on the effluent PO_4^{3-}-P concentration.

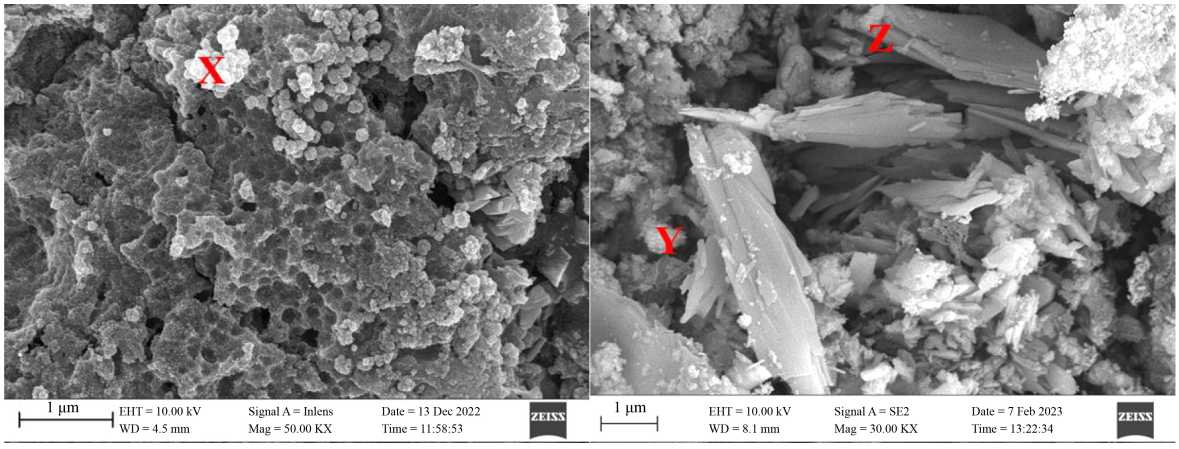

Fig. 4 SEM characterization of secondary minerals on the surface of fillers.

Table 2 EDS analysis of secondary minerals on the surface of pyrite particles

Element		C	N	O	Na	Al	Si	P	S	K	Ca	Fe
Percentage (%)	X	40.16	1.45	34.10	0.11	0.24	0.97	4.92	1.68	0.15	0.00	16.22
	Y	10.82	1.17	44.21	0.30	0.29	2.76	16.44	4.61	0.09	0.12	19.19
	Z	12.00	3.23	38.31	1.56	0.57	0.41	15.71	2.76	0.12	4.06	21.27

on the P atomic ratios and crystal appearance (Zhao, 2016; Ji, 2022) of the Y and Z positions, which was consistent with the results reported by Li et al. (2016).

3.1.3 Sulfate production investigation

SO_4^{2-} is an undesirable by-product of SAD techniques because it has a negative impact on water bodies; thus, SO_4^{2-} formation should be monitored throughout the operation of an SPSAD reactor. Effects of seasonal temperature shifts on sulfate production (i.e., ΔSO_4^{2-} = effluent SO_4^{2-} minus influent SO_4^{2-}) in the SPSAD reactor are shown in Fig. 5. The average sulfate production and nitrate removal rates were 192.86 and 29.74 mg/L at Stage I, 138.23 and 24.53 mg/L at Stage II, and 84.44 and 15.82 mg/L at Stage III. The average nitrate removal gradually decreased as the temperature decreased from Stage I to Stage III, meaning biological

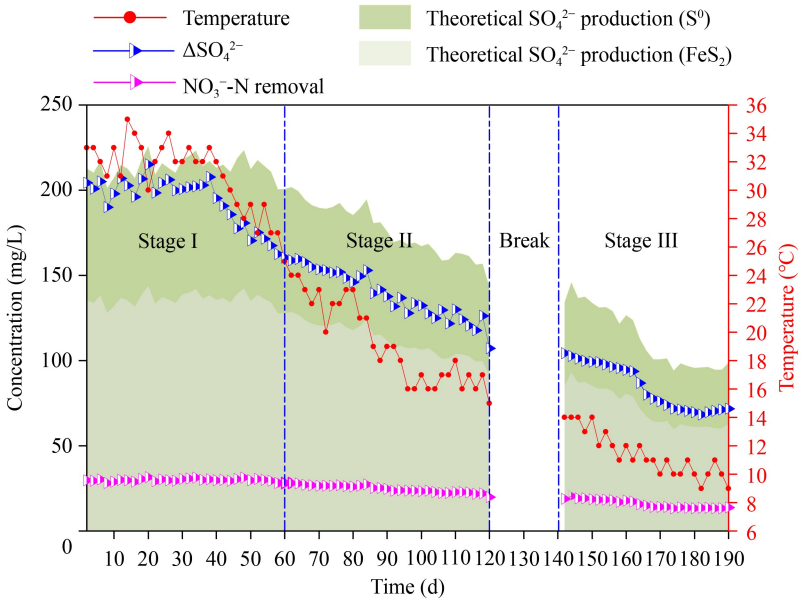

Fig. 5 Effects of seasonal temperature shifts on the SO_4^{2-} concentration in the SPSAD reactor.

denitrification was weakened by the low temperatures and resulted in the reduction of sulfate generation, as shown in Fig. 5. The decrease in average ΔSO_4^{2-} could be related to the increased proportion of denitrification by pyrite at low temperatures, where denitrification with pyrite as an electron donor produced less SO_4^{2-} than denitrification with the element S^0 as an electron donor. Alternatively, the reduction in sulfate production could be due to SRB (Sulfate Reducing Bacteria) in the autotrophic denitrification system, as presented in section 3.2.2 (Yang et al., 2017). As indicated in Fig. 5, after the 150th day at 9–11 °C, the ΔSO_4^{2-} was almost equal to the theoretical SO_4^{2-} production obtained by using pyrite as an autotrophic denitrification substrate. Ca^{2+} has been reported to react with SO_4^{2-} in water to form a slightly soluble precipitate (Kong et al., 2014). Notably, the XRF analysis showed that the fillers used in this study contained a certain amount of Ca^{2+} (mass percentage: 1.07%), as shown in Supporting Information. The size and mass of the ore particles gradually decreased as the experiment progressed as did the amount of Ca^{2+} leaching from the ore particles. The leached Ca^{2+} then reacted with the SO_4^{2-} to form $CaSO_4$ precipitation on the surface of the fillers, which is another possible reason for ΔSO_4^{2-} reduction.

$\Delta SO_4^{2-}/\Delta NO_3^-$-N denotes the increment of sulfate due to nitrate removal per unit mass. As indicated in Table 3, $\Delta SO_4^{2-}/\Delta NO_3^-$-N and NRL gradually decreased with decreasing temperatures. The ratio of $\Delta SO_4^{2-}/\Delta NO_3^-$-N was reported to be closely related to the denitrification contribution percentage of sulfur and pyrite. The denitrification percentage contributed by pyrite gradually increased from 35.55% to 74.18% as the temperature decreased (Lu, 2020), whereas the denitrification percentage contributed by pyrite gradually decreased from 64.45% to 25.82%. This result could be attributed to the different oxidation degrees of sulfur and ion pyrite, which were mainly due to differences in the ability and preference of microorganisms to utilize nutrients during the experimental process. Sulfur is easier to use than pyrite as the electron donor for denitrifying bacteria. After the reactor had been operating for an extended period of time, the number of denitrifying bacteria utilizing pyrite as an electron donor gradually increased. Additionally, pyrite was slowly dissolved by the H^+ produced from

Table 3 The averages SO_4^{2-} concentration, NRL, $\Delta SO_4^{2-}/\Delta NO_3^-$-N and denitrification contribution under three stages

Stage	Influent SO_4^{2-} (mg/L)	Effluent SO_4^{2-} (mg/L)	ΔSO_4^{2-} (mg/L)	ΔNO_3^--N (mg/L)	NRL (kg NO_3^--N/(m^3·d))	$\Delta SO_4^{2-}/\Delta NO_3^-$-N	Nitrogen removal contribution (%)	
							Element S^0	Pyrite
I	105.18	298.04	192.86	29.74	0.0595	6.48	64.45	35.55
II	124.30	262.53	138.23	24.53	0.0491	5.63	35.88	64.12
III	138.33	222.77	84.44	15.82	0.0316	5.34	25.82	74.18

the SAD process, which released more S^{2-} to be employed by the denitrifying bacteria. Specifically, in the early stage of experimental operation, sulfur was consumed first in the process of denitrification due to its own oxidation by oxygen gas; the fine sulfur particles flowed away with the effluent during long-term operation. Pyrite gradually decreased in size and increased in specific surface area as nitrate removal progressed in the reactor. Pyrite is easy to chemically oxidize and enhances its utilization by denitrifiers by accelerating the mass transfer between the aqueous phase and the biofilm. Changes in denitrification contribution indicated that the inhibitory effect of temperature on the S^0 autotrophic denitrification process was stronger than that on the pyrite autotrophic denitrification process. SAD-based reactors are less tolerant of low-temperatures and have difficultly adapting to large, prolonged shifts in temperature (Zhu and Chen, 2002). Although the proportion of denitrification performed by pyrite increased with decreasing temperatures, the NRL decreased from 0.0595 kg-N/(m^3·d) at Stage I to 0.0316 kg-N/(m^3·d) at Stage III. This result correlated with the changes in phosphorus removal, shown in Section 3.1.2. The decrease in temperature weakened the denitrification performance of pyrite, which reduced the effectiveness of both nitrogen and phosphorus removal.

3.2 Microbial community analysis

3.2.1 SEM characterization of filler's biofilm

The microscopic morphology of the sludge microorganisms on the surface of the reactor's fillers and the crystal configuration of several secondary minerals were characterized by scanning electron microscopy (SEM), as shown in Fig. 6. The reactor was dismantled at the end of the experiment (the 226th day), and the filler particles at the bottom of the reactor were immediately removed for SEM analysis. The fillers employed for SEM were taken from Stage III, the lowest temperature (9–12 °C), and the activity of the functional strains of nitrogen and phosphorus removal was largely suppressed, resulting in the deterioration of the denitrification performance of the SPSAD reactor. Several microorganisms were intolerant to cold and died. Thus, the biomass attached on the filler at Stage III was the minimum, and the Stage III SEM results were slightly inferior compared to those in Stages I and II with higher temperatures.

As indicated in the red box area in Fig. 6, at 50000 times magnification, many short-chain bacilli in singles and patches, which grew and multiplied in large quantities in the reactor, were observed on the surface of the ore particles. Additionally, in the blue box area, many bacteria with a medium-length and rod-like morphology were observed on the surface of the sulfide particles at 20000 times magnification. Sulfur autotrophic denitrifying functional bacteria (e.g., *Thiobacillus*) were in the shape of short rods or chains with a width of 0.5–0.8 μm and a length of 1.5–2.0 μm (Yang et al., 2018; Weng et al., 2022). In contrast, *Ferritrophicum*, a functional bacterium that oxidizes Fe^{2+} to Fe^{3+}, presented a rod-like morphology with a length of 0.9–1.7 μm and a width of 0.2–0.6 μm. Similarly sized microbes were observed in the SEM images in this study. Thus, it was speculated that the main functional bacteria species for denitrification and phosphorus removal in SPSAD increased in large quantities, and the filler performed well as a biocarrier for nitrogen and phosphorous removal. SEM was used to observe only the microbial micromorphology on the surface of the fillers; it failed to identify the microbial

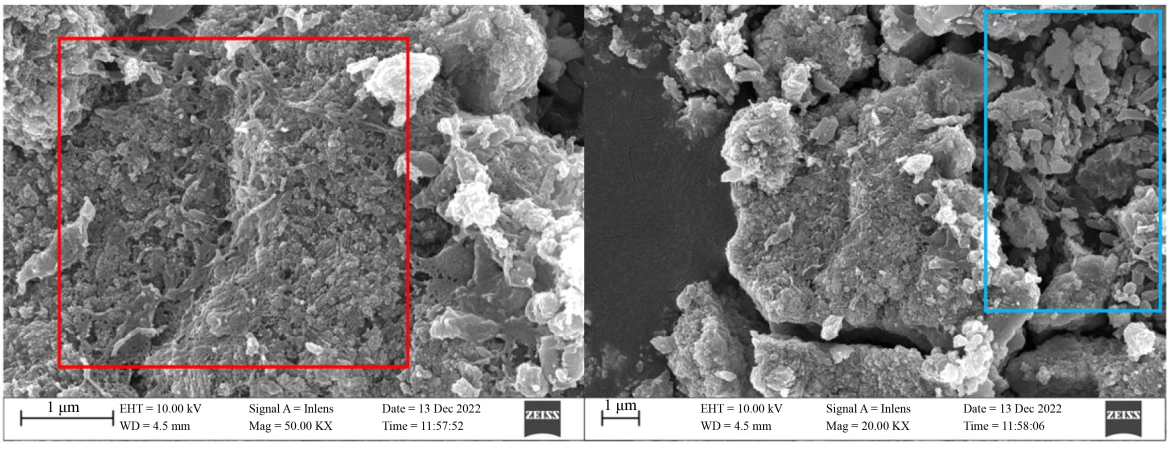

Fig. 6 SEM characterization of biofilms on the surface of the SPSAD filler.

species inside the reactor in detail. As such, a high-throughput sequencing analysis was performed to determine the effect of temperature on microbial community succession.

3.2.2 Effect of temperature on microbial community succession

To further explore the effects of seasonal temperature shifts on the nitrogen and phosphorus removal efficiency of the SPSAD reactor, the structures of the microbiological communities in the sludge samples collected from the bottom of the reactor on day 35 (32 °C) at Stage I, day 92 (19 °C) at Stage II, and day 190 (9 °C) at Stage III were investigated. At the phylum level, during the gradual decrease in temperature, *Proteobacteria*, *Chloroflexi*, *Bacteroidetes*, *Acidobacteriota* and *Actinobacteriota* were the main phyla in the SPSAD reactor, as shown in Fig. 7. Notably, *Proteobacteria* was the dominant phylum with the highest percentage (> 42.68%) in all three temperature stages. As the temperature decreased, the abundances of *Proteobacteria* and *Chloroflexi* decreased from 62.84% and 6.71% to 42.68% and 5.17%, respectively, and the abundances of *Actinobacteriota*, *Firmicutes* and *Desulfobacterota* increased from 3.49%, 1.40%, and 1.21% to 10.55%, 5.78%, and 4.77%, respectively. No significant changes were observed for the remaining phyla. The abundances of *Actinobacteriota*, *Firmicutes* and *Desulfobacterota* distinctly increased, whereas the abundances of *Proteobacteria* and *Chloroflexi* substantially decreased. Many typical nitrate-reducing and iron-oxidizing bacteria belong to *Proteobacteria* (Zhang et al., 2022), and the significant decrease in their abundance was the main reason for the deterioration in the nitrogen and phosphorus removal performance. *Bacteroidota* and *Acidobacteriota* play an important role in nitrogen and phosphorous removal. Bacteroidota are produced in the anaerobic denitrification process by degrading high organic compounds to reduce nitrate. *Acidobacteriota* is capable of oxidizing Fe^{2+} to Fe^{3+} using O_2 as an electron acceptor, which facilitates phosphorus removal. In summary, the results showed that the seasonal temperature shifts affected the phyla of the reactor, with significant impact observed on abundance.

As shown in Fig. 8, a total of 20 genera were detected (> 1% detection limit) in each of the three stages. Different microorganisms have different abilities to resist low temperature conditions, and their growth and reproduction differ under different temperature environments. The optimum growth temperature of microorganisms involved in SAD technology is reported to be 28–30 °C (Zhou et al., 2011; Fajardo et al., 2014; Di Capua et al., 2016). The abundance of the dominant genera in the SPSAD reactor significantly changed due to seasonal temperature variations. The abundance of *Thiobacillus* was the highest among the 20 genera and was the main functional microorganism in the SPSAD reactor, which was consistent with the results of Wang et al. (2019). Thiobacillus, a parthenogenetic anaerobic and specialized autotroph, is a common microorganism in sulfur autotrophic denitrification systems. As the main denitrifying functional bacteria in the system, their number changed with the temperature, which impacted the efficiency of

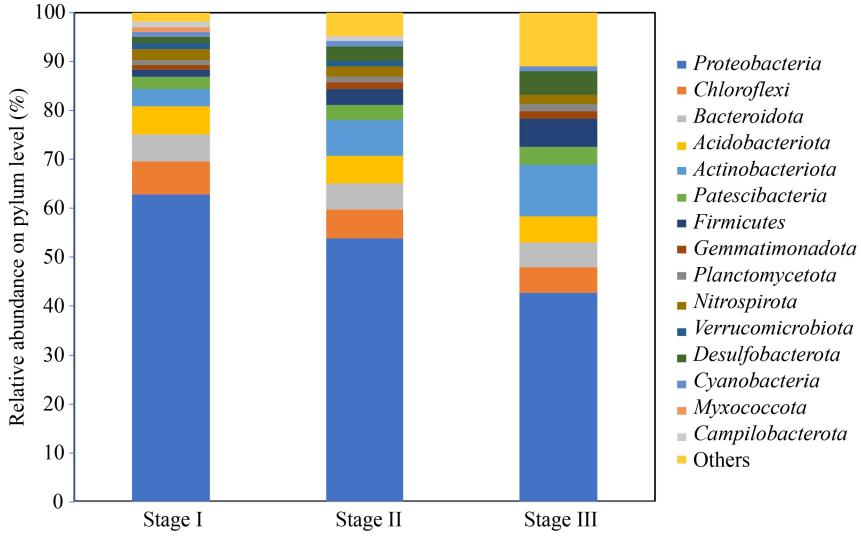

Fig. 7 Effects of seasonal temperature shifts on microbial community structure at the phylum level.

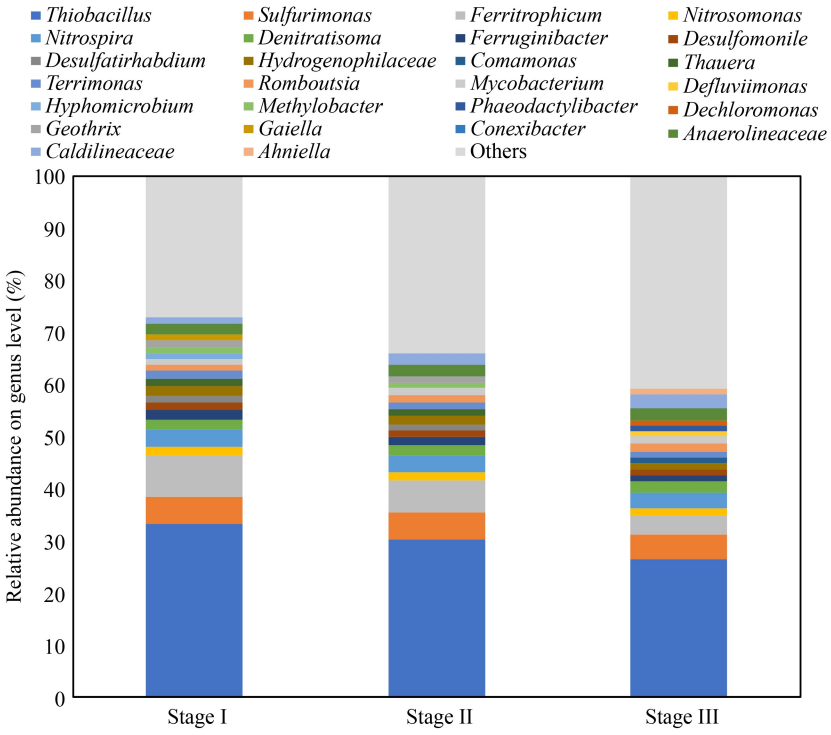

Fig. 8 Effects of seasonal temperature shifts on microbial community structure at the genus level.

the denitrification and nitrogen removal. Genera in the *Proteobacteria* were the dominant species during the entire operation of the SPSAD reactor. The number of genera belonging to *Proteobacteria* was 8, 8 and 9, corresponding to Stages I, II, and III, respectively. The remaining genera belonged to the *Chloroflexi*, *Acidobacteriota*, and *Bacteroidota*.

At the genetic level, *Thiobacillus*, *Sulfurimonas*, *Ferritrophicum*, *Nitrospira,* and *Nitrosomonas* decreased from 33.18%, 5.2%, 7.8%, 3.34%, and 1.81% to 26.44%, 4.62, 3.6%, 3.11%, and 1.42%, respectively. *Thiobacillus* and *Sulfurimonas* are typical sulfur autotrophic denitrifying bacteria that play crucial roles in inorganic sulfur oxidation and nitrate reduction (Lu et al., 2010). The combined abundance of *Thiobacillus* and *Sulfurimonas* decreased from 38.38% in Stage I to 31.06% in Stage III. The decrease in their abundance was closely associated with the deterioration in nitrogen removal performance during the low temperature stages. In addition, the abundance of *Ferritrophicum* (i.e., an iron-oxidizing bacteria) decreased from 7.80% to 3.60% under low temperatures, which could have contributed to the level of influent PO_4^{3-} remaining low, at 0.4–0.8 mg/L, for an extended period of time. *Ferruginibacter*, which is able to decompose some organic substances into small molecular organics and participate in the iron metabolic cycle to accelerate the conversion between Fe^{2+} and Fe^{3+}, was also detected in the reactor (Wang et al., 2012). The combined abundances of *Ferritrophicum* and *Ferruginibacter* decreased from 9.6% to 4.6%. Subsequently, the amount of Fe^{3+} produced by *Ferritrophicum* and *Ferruginibacter* decreased, which contributed to the poor PO_4^{3-} removal under low temperatures.

Nitrosomonas (AOB functional bacterium) and *Nitrospira* (NOB functional bacterium) were detected in the sludge, which was consistent with the pathway of NH_4^+-N removal in this study (NH_4^+-N→NO_2^--N→NO_3^--N). As the reactor progressed from 25–35 °C to 9–11 °C, the abundances of *Nitrosomonas* and *Nitrospira* slightly decreased from 1.81% and 3.34% to 1.42% and 3.11%, respectively. Enrichment of *Nitrospira* was reported in an autotrophic denitrification filter using pyrite as an electron donor by Xu et al. (2022). The reactor had a certain oxidation capacity for NH_4^+-N during the low temperature stages, thus the removal rate of NH_4^+-N remained at approximately 44.24% instead of accumulating. In addition to autotrophic denitrifying bacteria, heterotrophic denitrifying bacteria, including *Thauera* (1.5% abundance in Stage I), *Comamonas* (1.13% abundance in Stage III), *Denitratisoma* (abundance increased from 1.9% to 2.2% during Stage III) and *Desulfomonile*

(abundance decreased from 1.48% to 1.09% during Stage III), were present in the SPSAD reactor. The abundance of *Desulfatirhabdium* was 1.16% at Stage I, which could reduce SO_4^{2-} to S^{2-} or H_2S under anaerobic conditions and is responsible for SO_4^{2-} production reduction in the effluent. It was reported that *Thauera* can facilitate the production of the extracellular polymer TB-EPS, which contributes to cell aggregation and floc formation (Geng, 2021). Overall, the succession in the microbial community structure was influenced by exposure to different temperature conditions, which resulted in the varying nitrate and phosphorus removal abilities of our SPSAD reactor.

3.3 Removal mechanism analysis

As indicated in Fig. 9, the pollutant removal pathway and electron transfer process in the reactor were derived from the pollutant removal performance, the SEM-EDS results of the fillers and the microbial diversity analysis. The *narG*, *nirK*, *norB*, and *nosZ* enzymes are responsible for reducing NO_3^--N, NO_2^--N, NO, and N_2O, respectively, in SAD-based systems (Feng et al., 2024; Wang et al., 2025). The influent NH_4^+-N was removed from the reactor by converting it into NO_3^--N in two steps. NH_4^+-N was first converted to NO_2^--N by *Nitrosomonas* and then converted to NO_3^--N by *Nitrospira*. The total NO_3^--N was equal to the influent NO_3^--N plus the converted NO_3^--N from the influent NH_4^+-N. The total NO_3^--N gradually converted to N_2 by obtaining electrons from sulfur/pyrite, which were removed by two main functional bacteria (i.e., *Thiobacillus* and *Sulfurimonas*). The NO_3^--N to NO_2^--N reduction process is the primary step for denitrification, and a higher relative abundance of the narG coding gene is advantageous for increased nitrate reduction (Ma et al., 2024). Similarly, the pyrite-based autotrophic denitrification process employed in this study had abundant narG coding genes (Zhao et al., 2022). Notably, NO_2^--N accumulated in the reactor if the reaction from NO_3^--N to N_2 was incomplete. Electrons from the element S^0 and pyrite were oxidized to SO_4^{2-}, and a part of SO_4^{2-} was converted to sulfide S^{2-} or a low-valence sulfur with sulfate-reducing bacteria (SOB), such as *Desulfomonile* and *Desulfatirhabdium*. The results above detail nitrogen removal in the SPSAD reactor. The pyrite ore generated a large amount of Fe^{2+} during the reaction with nitrate; the released Fe^{2+} were then oxidized to Fe^{3+}, which released the electrons for denitrification with *Ferritrophicum* and *Ferruginibacter*. The results of secondary mineral EDS analysis revealed that some Fe^{3+} reacted with OH^- to form $Fe(OH)_3$ precipitation, while some Fe^{3+} and Ca^{2+} reacted with the influent PO_4^{3-} to form $FePO_4$ and $CaHPO_4$ precipitation to remove PO_4^{3-}. Additionally, $Fe(OH)_3$ acted as a flocculant to further reduce the content of the effluent PO_4^{3-}. The SEM-EDS results of the filler demonstrated that the plate-like $FePO_4$ precipitation was clearly attached to the surface of the ore particles. The abundances of *Nitrosomonas*, *Nitrospira*, *Thiobacillus*, *Sulfurimonas*, *Desulfomonile*, *Desulfatirhabdium*, *Ferritrophicum*, and *Ferruginibacter* decreased when the operation of the SPSAD reactor changed from Stage I to Stage III. Accordingly, nitrification, denitrification, sulfate reduction and phosphorus removal in the SPSAD reactor decreased, which caused an increase in effluent NH_4^+-N, NO_2^--N, NO_3^--N, SO_4^{2-}, and PO_4^{3-}-P.

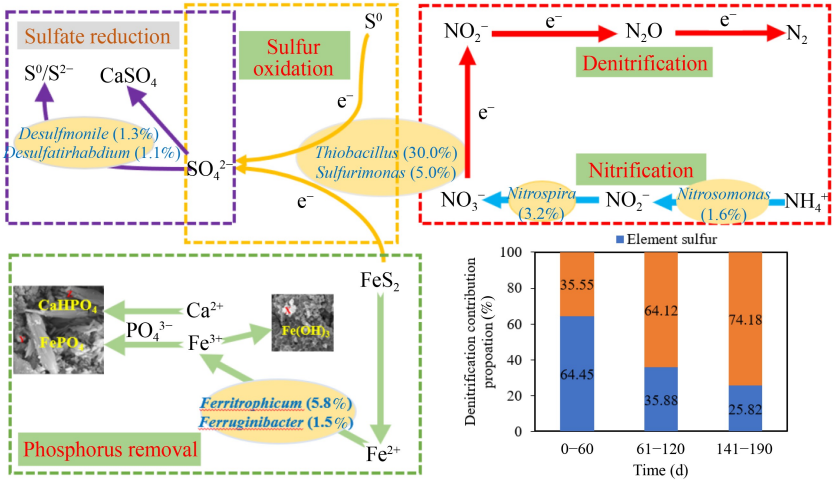

Fig. 9 Removal mechanism of nitrogen and phosphorus in the SPSAD reactor.

3.4 The feasibility of practical application

Appropriate temperature control is essential to ensure the efficient and stable operation of SAD-based systems. To achieve stable operation, it is important to understand the impact of temperature fluctuations on the SPSAD reactor and develop feasible control strategies. In this study, comparing the correlations between temperature, nitrogen and phosphorous removal and microbial activities revealed the following key information. First, seasonal temperature variations greatly impact PO_4^{3-}-P removal; the removal rate of PO_4^{3-}-P gradually decreased at low temperatures. However, the concentration of influent PO_4^{3-}-P was 0.4–0.75 mg/L, and the effluent PO_4^{3-}-P remained in the range of 0.15–0.48 mg/L (less than 0.5 mg/L), which satisfies the discharge standards for pollutants from municipal wastewater treatment plants in China (i.e., GB18918-2002). Second, the proportion of denitrification driven by pyrite increased as temperature decreased, and the SO_4^{2-} yield ($\Delta SO_4^{2-}/\Delta NO_3^{-}$-N ratio of 5.52) significantly decreased compared to the yield of S^0 ($\Delta SO_4^{2-}/\Delta NO_3^{-}$-N ratio of 7.54). This finding implied that the constructed SPSAD reactor was advantageous for SO_4^{2-} removal. In addition, the optimum temperature for *Thiobacillus*, the main functional microorganism of the SPSAD, to achieve maximum nitrogen removal efficiency was 30–35 °C (Liu et al., 2023). Maintaining an optimal water temperature for the primary functional microorganism (30–35 °C) would inevitably cause heat loss during the application of SPSAD for the treatment of secondary effluent at low temperatures. Heating the effluent above 30°C consumes large quantities of heat energy, which significantly increases the operating cost. Thus, enhancing reactor performance by increasing the operating temperature is not a practical solution. Although the nitrogen removal efficiency gradually decreased with temperature, the NRL of the SPSAD was stable under a certain loading (Fig. 2). In addition, the practical application of denitrification under cold weather conditions could be enhanced by adding a carbon source and microbial strains. In general, the effluent water quality quickly deteriorated when the temperature decreased to 9–12 °C. However, the NRL of the SPSAD reactor reached 0.0316 kg NO_3^{-}-N/(m^3·d) during the lowest temperature period, which was an excellent performance in comparison to other SAD studies (Fajardo et al., 2014; Xu et al., 2019; Li et al., 2020c) at low temperatures (10–12 °C). When the temperature was reduced to 9–12 °C, the concentration of effluent NO_3^{-}-N was less than 15 mg/L, and the removal rate was greater than 42%. *Nitrosomonas* and *Nitrospira* remained in the SPSAD reactor, with abundances that slightly decreased as the temperature shifted from 35 to 9 °C. Free ammonia does not accumulate in large quantities, thus alleviating the inhibition of nitrate oxidation by free ammonia in the system. This reactor is suitable for the nitrogen removal treatment of actual secondary effluent at low temperatures. This system can greatly reduce the demand for organic carbon compared with the traditional heterotrophic denitrification process and is a relatively cost-effective nitrogen removal technology at low temperatures. Therefore, the constructed SPSAD system could be employed for the nitrogen removal treatment of actual secondary effluent in cold areas.

4 Conclusions

In this study, a composite substrate autotrophic reactor (SPSAD) was constructed by mixing element S^0 and pyrite in hollow plastic balls that were used as filler. The denitrification performance, phosphorus removal, and microbial community succession under long-term seasonal variations (190 d in total) of the SPSAD reactor were systematically investigated. Important findings include: (1) the synergistic substrate composed of S^0 and pyrite enhanced the resilience of the SPSAD reactor to temperature variations; (2) as the temperature shifted from 35 to 9 °C, the NRE and PO_4^{3-}-P removal rates decreased from 93.2% and 67.9% to 49.9% and 30.2%, respectively; (3) the average NRL changed from 0.060 to 0.032 kg NO_3^{-}-N/(m^3·d); (4) although NO_2^{-}-N did not substantially accumulate in Stage I, the amount of NO_2^{-}-N accumulation increased from 0.34 mg/L in Stage II to 1.10 mg/L in stage III; (5) the inhibitory effect triggered by low temperatures on *NirS* was stronger than that triggered by the NO_3^{-}-N reductase lineage. Thus, the constructed SPSAD reactor was effective at simultaneously removing nitrogen and phosphorous at low temperatures. In addition, the SEM-EDS results of the fillers revealed that amorphous $Fe(OH)_3$ and irregular plate-like $FePO_4$ and $CaHPO_4$ aggregates were responsible for PO_4^{3-}-P removal by chemical precipitation. Biological denitrification was weakened by the low temperatures, resulting in a reduction in sulfate generation. the decrease in ΔSO_4^{2-} was close to the increased proportion of denitrification by pyrite at low temperatures because denitrification with pyrite as an electron donor produced less SO_4^{2-} than denitrification with the element S^0. Microbial community structure analysis revealed that the abundance of microbes at the phylum and genus levels gradually decreased with decreasing temperature. With

an average abundance of 53.11%, *Proteobacteria* were the chief phylum in the reactor; other phyla accounted for less than 7.13%. *Thiobacillus* was significantly enriched and was the predominant genera in denitrification. Overall, the developed SPSAD reactor proved feasible and adaptable for simultaneous N and P removal from practical municipal secondary effluent under low temperature conditions.

CRediT Authorship Contribution Statement

Chuanyi Zhang: Writing-original draft, Methodology, Data curation, Conceptualization. **Zhiping Zhu:** Writing-review and editing, Visualization, Data curation. **Limei Yuan:** Project administration, Validation, Investigation. **Daxin Yang:** Investigation, Validation, Data curation. **Qiang Xu:** Formal analysis, Writing-review and editing, Investigation. **Sijie Ge:** Writing-review and editing, Supervision, Visualization, Conceptualization, Formal analysis, Funding acquisition.

Conflict of Interests The authors declare that they have no known competing financial interests or personal relationships that could have appeared to influence the work reported in this paper.

Acknowledgements This study was supported by the National Natural Science Foundation of China (Nos. 52400145, 51974314, and 52270171), the Special Project on Bases and Talents of the Ministry of Science and Technology of China (No. 2022XJKK1004) and the Fundamental Research Funds for the Central Universities of China (No. 2019XKQYMS79).

Electronic Supplementary Material Supplementary material is available in the online version of this article at https://doi.org/10.1007/s11783-025-2002-y and is accessible for authorized users.

References

Chen D, Wang H Y, Yang K, Ma F (2018). Performance and microbial communities in a combined bioelectrochemical and sulfur autotrophic denitrification system at low temperature. Chemosphere, 193: 337–342

Chen X Y, Yang L, Chen F, Song Q N, Feng C P, Liu X, Li M (2022). High efficient bio-denitrification of nitrate contaminated water with low ammonium and sulfate production by a sulfur/pyrite-based bioreactor. Bioresource Technology, 346: 126669

Chen Z Q, Pang C, Wen Q X (2023). Coupled pyrite and sulfur autotrophic denitrification for simultaneous removal of nitrogen and phosphorus from secondary effluent: feasibility, performance and mechanisms. Water Research, 243: 120422

Cui P, Wan N H, Li C Y, Zou L, Ma M, Du J, Jiang Y (2024). Comparative analysis of sulfur-driven autotrophic denitrification for pilot-scale application: pollutant removal performance and metagenomic function. Bioresource Technology, 413: 131433

Di Capua F, Ahoranta S H, Papirio S, Lens P N L, Esposito G (2016). Impacts of sulfur source and temperature on sulfur-driven denitrification by pure and mixed cultures of *Thiobacillus*. Process Biochemistry, 51(10): 1576–1584

Demir Ö, Atasoy A D, Çalış B, Çakmak Y, Capua F D, Sahinkaya E, Uçar D. Impact of temperature and biomass augmentation on biosulfur-driven autotrophic denitrification in membrane bioreactors treating real nitrate-contaminated groundwater. Science of the Total Environment, 2021, 853: 158470

Fajardo C, Mora M, Fernández I, Mosquera-Corral A, Campos J L, Méndez R (2014). Cross effect of temperature, pH and free ammonia on autotrophic denitrification process with sulphide as electron donor. Chemosphere, 97: 10–15

Feng L J, Sun X R, Wang J Q, Xie T N, Wu Z L, Xu J K, Wang Z Y, Yang G F (2024). Performance and microbial mechanism in sulfide-driven autotrophic denitrification by different inoculation sources in face of various sulfide and sulfate stress. Bioresource Technology, 413: 131443

Geng Y W (2021). Application of a Novel Sulfur Autotrophic Denitrification Reactor for Advanced Denitrification. Dissertation for the Doctoral Degree. Suzhou: Suzhou University of Science and Technology (in Chinese)

Hu H D, Shi Y J, Liao K W, Ma H J, Xu K, Ren H Q (2019). Effect of temperature on the characterization of soluble microbial products in activated sludge system with special emphasis on dissolved organic nitrogen. Water Research, 162: 87–94

Ji X Y (2022). Study on Preparation of Anhydrous Calcium Hydrogen Phosphate by Micro-Impinging Stream Reactors and its Application Properties. Thesis for the Masteral Degree. Beijing: Beijing University of Chemical Technology (in Chinese)

Kim J H, Guo X J, Park H S (2008). Comparison study of the effects of temperature and free ammonia concentration on nitrification and nitrite accumulation. Process Biochemistry, 43(2): 154–160

Kong Z, Feng C P, Chen N, Tong S, Zhang B G, Hao C B, Chen K (2014). A soil infiltration system incorporated with sulfur-utilizing autotrophic denitrification (SISSAD) for domestic wastewater treatment. Bioresource Technology, 159: 272–279

Li H B, Li Y F, Guo J B, Song Y Y, Hou Y N, Lu C C, Han Y, Shen X F, Liu B W (2021). Effect of calcinated pyrite on simultaneous ammonia, nitrate and phosphorus removal in the BAF system and the Fe^{2+} regulatory mechanisms: electron transfer and biofilm properties. Environmental Research, 194: 110708

Li H Y, Xu Y H, Dong H, Min J, Xu H Y, Sun D Z, Liu X Y, Dang Y, Qiu B, Mennella T, et al. (2024). Evidence of autotrophic direct electron transfer denitrification (DETD) by *Thiobacillus* species enriched on biocathodes during deep polishing of effluent from a municipal wastewater treatment plant. Chemical Engineering Journal, 495: 153389

Li R H, Morrison L, Collins G, Li A M, Zhan X M (2016). Simultaneous nitrate and phosphate removal from wastewater lacking organic matter through microbial oxidation of pyrrhotite coupled to nitrate reduction. Water Research, 96: 32–41

Li R H, Wei D Y, Wang W, Zhang Y W (2020a). Pyrrhotite-sulfur autotrophic denitrification for deep and efficient nitrate and phosphate removal: synergistic effects, secondary minerals and microbial community shifts. Bioresource Technology, 308:

123302

Li T, Gao Y L, Tang Y Y, Xu Y J, Ren H Q, Huang H (2022). A new LDH based sustained-release carbon source filter media to achieve advanced denitrogenation of low C/N wastewater at low temperature. Science of the Total Environment, 838: 156488

Li Y F, Guo J B, Li H B, Song Y Y, Chen Z, Lu C C, Han Y, Hou Y N (2020b). Effect of dissolved oxygen on simultaneous removal of ammonia, nitrate and phosphorus via biological aerated filter with sulfur and pyrite as composite fillers. Bioresource Technology, 296: 122340

Li Y Y, Wang Y L, Wan D J, Li B, Zhang P Y, Wang H J (2020c). Pilot-scale application of sulfur-limestone autotrophic denitrification biofilter for municipal tailwater treatment: performance and microbial community structure. Bioresource Technology, 300(C): 122682

Lin Q, De Vrieze J, Li J B, Li X Z (2016). Temperature affects microbial abundance, activity and interactions in anaerobic digestion. Bioresource Technology, 209: 228–236

Liu H, Zeng W, Fan Z W, Li J M, Zhan M J, Peng Y Z (2021). Effect of iron on enhanced nitrogen removal from wastewater by sulfur autotrophic denitrification coupled to heterotrophic denitrification under different substrate ratios. Chemical Engineering Journal, 421: 129828

Liu X Z, Zhao C S, Xu T T, Liu W, Chen Q F, Li L Z, Tan Y, Wang X K, Dong Y N (2023). Pyrite and sulfur-coupled autotrophic denitrification system for efficient nitrate and phosphate removal. Bioresource Technology, 384: 129363

Lu N N (2020). Performance of Nitrogen and Collaborative Phosphorus Removal via Composite Sulfur Substrate Autotrophic Denitrification. Thesis for the Masteral Degree. Xuzhou: China University of Mining and Technology (in Chinese)

Lu S P, Gischkat S, Reiche M, Akob D M, Hallberg K B, Küsel K (2010). Ecophysiology of Fe-cycling bacteria in acidic sediments. Applied and Environmental Microbiology, 76(24): 8174–8183

Lv X, Zhang W X, Deng J S, Feng S Y, Zhan H Z (2024). Pyrite and humus soil-coupled mixotrophic denitrification system for efficient nitrate and phosphate removal. Environmental Research, 247: 118105

Ma W J, Zhang H M, Ma Z S, You X J, Wei X Y, Li Y, Tian Y (2024). Meta-analyzing the mechanism of pyrogenic biochar strengthens nitrogen removal performance in sulfur-driven autotrophic denitrification system: evidence from metatranscriptomics. Water Research, 253: 121296

Meynet P, Joss A, Davenport R J, Fenner K (2024). Impact of long-term temperature shifts on activated sludge microbiome dynamics and micropollutant removal. Water Research, 258: 121790

Miu B, Jiang Y, Liu P P, Wang D L, Hao W, Liang P, Huang X (2019). Effect of low temperature on sulfur autotrophic denitrification and its improvement. China Water & Wastewater,35(5): 105–109 (in Chinese)

Panswad T, Doungchai A, Anotai J (2003). Temperature effect on microbial community of enhanced biological phosphorus removal system. Water Research, 37(2): 409–415

Sahinkaya E, Dursun N, Kilic A, Demirel S, Uyanik S, Cinar O (2011). Simultaneous heterotrophic and sulfur-oxidizing autotrophic denitrification process for drinking water treatment: control of sulfate production. Water Research, 45(20): 6661–6667

Shi M, Li X, Dang P Z, Xu Q, Huang T Y, Yuan Y, Huang Y, Zhou C (2024). Effects of O_2 on accumulation of nitrous and elemental sulfur and microbial community structure in double short-cut sulfur autotrophic denitrification system. Bioresource Technology, 409: 131243

Wang S Q, Yuan Y, Liu F, Liu R D, Zhang X Z, Jiang Y B (2025). Coupling thiosulfate-driven denitrification and anammox to remove nitrogen from actual wastewater. Bioresource Technology, 417: 131840

Wang T, Li X, Wang H, Xue G, Zhou M D, Ran X C, Wang Y Y (2023). Sulfur autotrophic denitrification as an efficient nitrogen removals method for wastewater treatment towards lower organic requirement: a review. Water Research, 245: 120569

Wang T, Wang H, Ran X C, Wang Y Y (2024). Salt stimulates sulfide-driven autotrophic denitrification: microbial network and metagenomics analyses. Water Research, 257: 121742

Wang W, Wei D Y, Li F C, Zhang Y W, Li R H (2019). Sulfur-siderite autotrophic denitrification system for simultaneous nitrate and phosphate removal: from feasibility to pilot experiments. Water Research, 160: 52–59

Wang X H, Hu M, Xia Y, Wen X H, Ding K (2012). Pyrosequencing analysis of bacterial diversity in 14 wastewater treatment systems in China. Applied and Environmental Microbiology, 78(19): 7042–7047

Weng Z S, Ma H, Ma J, Kong Z, Shao Z, Yuan Y, Xu Y, Ni Q, Chai H (2022). Corncob-pyrite bioretention system for enhanced dissolved nutrient treatment: carbon source release and mixotrophic denitrification. Chemosphere, 306: 135534

Xu B K, Shi L S, Zhong H, Wang K (2019). The performance of pyrite-based autotrophic denitrification column for permeable reactive barrier under natural environment. Bioresource Technology, 290: 121763

Xu Z S, Li Y N, Zhou P P, Song X S, Wang Y H (2022). New insights on simultaneous nitrate and phosphorus removal in pyrite-involved mixotrophic denitrification biofilter for a long-term operation: performance change and its underlying mechanism. Science of the Total Environment, 845: 157403

Yang D X, Zhang C Y, Ge S J, Xie Y Q, Yuan L M (2024). Performance of single PN/A reactor under wide fluctuation of nitrogen load. Environmental Science and Pollution Research International, 31: 58083–58092

Yang Y, Chen T H, Morrison L, Gerrity S, Collins G, Porca E, Li R H, Zhan X M (2017). Nanostructured pyrrhotite supports autotrophic denitrification for simultaneous nitrogen and phosphorus removal from secondary effluents. Chemical Engineering Journal, 328: 511–518

Yang Y, Chen T H, Zhang X, Qing C S, Wang J, Yue Z B, Liu H B, Yang Z (2018). Simultaneous removal of nitrate and phosphate from wastewater by siderite based autotrophic denitrification. Chemosphere, 199: 130–137

Zhang X X, Hu X L, Zhang L, Wang H Y (2022). Effect of HRT on operation performance of sulfur/siderite autotrophic denitrification system. Industrial of Water Treatment, 42(11): 177–183 (in Chinese)

Zhang Y W (2018). Study of the Behavior and Mechanism of Nitrogen and Phosphorus Removal in Wastewater by Pyrite. Dissertation for the Doctoral Degree. Nanjing: Nanjing University (in Chinese)

Zhao L F, Xue L Y, Wang L, Liu C, Li Y (2022). Simultaneous heterotrophic and FeS_2-based ferrous autotrophic denitrification process for low-C/N ratio wastewater treatment: nitrate removal performance and microbial community analysis. Science of the Total Environment, 829: 154682

Zhao N N (2016). Study on Synthesis Process Optimization and Performance of $FePO_4$. Dissertation for the Doctoral Degree. Tianjin: Hebei University of Technology (in Chinese)

Zhou J M, Ding L, Cui C Z, Lindeboom R E F (2024). High nitrite accumulation in hydrogenotrophic denitrification at low temperature: transcriptional regulation and microbial community succession. Water Research, 263: 122144

Zhou W L, Sun Y J, Wu B T, Zhang Y, Huang M, Miyanaga T, Zhang Z J (2011). Autotrophic denitrification for nitrate and nitrite removal using sulfur-limestone. Journal of Environmental Sciences, 23(11): 1761–1769

Zhu S M, Chen S L (2002). The impact of temperature on nitrification rate in fixed film biofilters. Aquacultural Engineering, 26(4): 221–237

Zuo F M, Sui Q W, Yu D W, Zhang J Y, Gui S L, Wang Y Y, He Y W, Wei Y S (2024). A temperature-resilient anammox process for efficient treatment of rare earth element tailings wastewater via synergistic nitrite supply of partial nitritation and partial denitrification. Bioresource Technology, 407: 131111